BMC Infectious Diseases

RESEARCH Open Access

Traffic-driven spatio-temporal prediction for fine-scale epidemic outbreaks in China

Han Li[1,2], Jianping Huang[1,2*], Wei Yan[1,2], Zihan Hao[1,2], Rui Wang[1,2], Yingjie Zhao[1,2], Shujuan Hu[1,2], Xinbo Lian[1,2,3] and Licheng Li[1,4]

Abstract

Background As the high connectivity creates favorable conditions for the infectious diseases, understanding the dynamics of epidemic spread across regions is significant. However, existing models often focus on single dimensions and specific factors under strict controls, but generally overlook regional differences and interactions.

Methods In this research, we constructed a spatio-temporal forecasting model based on multiple modeling architectures, specifically designed to predict the post-lockdown epidemic's transmission at a fine scale across prefecture-level cities nationwide. The model integrates comprehensive factors and constructs a structured graph based on transportation patterns and characteristic variables across municipal regions in China. To further enhance its ability to capture spatial interactions among regions, the model integrates human mobility into edge weight calculations to optimize the adjacency matrix.

Results We analyzed the prediction errors across different urban clusters, provinces, folds, and forecast durations, revealing spatial variations and consistent error reductions. The results demonstrate that our model can accurately predict the spatio-temporal spread of the epidemic across 309 Chinese prefecture-level cities with a high correlation coefficient ($r = 0.94$) validated through extensive cross-validation.

Conclusions Our proposed approach integrates transportation patterns and human mobility into edge weight calculations to enhance spatial connectivity. This post-lockdown simulation across cities in China offers a fine-grained analytical scale previously unexplored, and the comprehensive analysis provides enhanced insights into epidemic dynamics and transmission patterns, supporting the future public health strategies.

Keywords Spatio-temporal prediction, Epidemic spread, Transportation patterns, Human mobility

*Correspondence:
Jianping Huang
hjp@lzu.edu.cn
[1]Collaborative Innovation Center for Western Ecological Safety, College of Atmospheric Sciences, Lanzhou University, Lanzhou 730000, China
[2]College of Atmospheric Sciences, Lanzhou University, Lanzhou 730000, China
[3]College of Earth and Environmental Sciences, Lanzhou University, Lanzhou 730000, China
[4]School of Mathematics and Statistics, Lanzhou University, Lanzhou 730000, China

Introduction

Since COVID-19 began spreading globally, its profound impacts on public health, economy, and social life have made it one of the most severe public health crises in recent history [1, 2]. Driven by global climate change and human activities, significant shifts in the spread of the pandemic are anticipated [3, 4]. The COVID-19 pandemic has underscored the urgent need for more effective tools to assess and predict the spread and intensity of epidemics across different regions [5]. Furthermore, the complexity of the pandemic is exacerbated by the interaction of various factors, especially human mobility, along with socioeconomic conditions, public health conditions, and meteorological factors all contribute to the increased complexity of the pandemic [6–8].

On December 7, 2022, the General Office of the State Council of China issued new regulations to further optimize epidemic prevention and control measures, explicitly canceling mass nucleic acid testing, nucleic acid certificate inspections, as well as travel and health codes [9]. This shift brings new challenges, particularly in the context of increased mobility, which is a critical factor in the spread of epidemics [6]. Large-scale mobility between communities or regions can transport the virus from high-risk to low-risk areas, increasing the risk of wider geographical spread and potentially triggering new outbreaks [10–12]. Especially when the relaxation of control measures led to increased transportation activity, posing new public health challenges. Studies using traffic flow data for analysis indicate that this high-intensity flow of people greatly increases the likelihood of cross-regional virus transmission [13, 14]. The research also shows that public transportation accelerates the spread of COVID-19, especially when travelers from high-incidence areas introduce the virus to less affected regions, initiating new transmission chains [15]. Following the adjustment of control measures, many areas in China quickly reached their infection peaks, with the first wave reportedly peaking in late December 2022 and subsequently declining [16]. After the relaxation of epidemic policies, the specific social behaviors and mobility patterns continue to play a pivotal role in shaping the spatio-temporal distribution characteristics of the epidemic.

In the field of infectious disease epidemiology, the Susceptible-Exposed-Infectious-Recovered (SEIR) model is widely used to predict and analyze the dynamics of disease transmission. This model describes the changes in populations over time using differential equations, including key parameters such as the infection rate, recovery rate, and incubation period [17]. Consequently, the traditional SEIR model has been enhanced by incorporating a variety of parametrization schemes under different scenarios for more realistic simulations, and these improved models have achieved high prediction accuracy in epidemic forecasting [18–21]. Meanwhile, the SEIR models often focus on internal infection rates, neglecting human mobility and spatial distribution, which limits their effectiveness in spatially diverse scenarios. Some improved SEIR models also incorporate transmission dynamics within transportation systems and parameters for inter-regional human mobility, significantly enhancing the accuracy of predicting epidemic spread risks during holidays [22–28]. It is evident that the changing mobility patterns transform epidemic simulation into a complex spatio-temporal challenge, necessitating advanced models that can handle the intricate interplay of temporal dynamics and spatial heterogeneity.

In recent years, the rapid advancement of deep learning has significantly improved the technical ability to model complex spatio-temporal dynamics in infectious diseases. Among the various methodologies, Graph Neural Networks (GNNs) have gained substantial popularity across diverse fields. By leveraging the intricate relationships between nodes and edges, GNNs excel at capturing complex network structural features [29]. Using GNNs to model the spread of epidemics can more accurately consider the impacts of geographical and social network structures, thereby improving the accuracy and applicability of predictions [30, 31]. To further enhance their predictive power, GNNs are frequently integrated with time series models, allowing for the simultaneous capture of both spatial and temporal dependencies. Time series data, in particular, provide a means to observe and analyze how diseases evolve over time, enabling the identification of trends and dynamic patterns. A notable advancement in time series modeling is the development of Long Short-Term Memory Networks (LSTMs), which were specifically designed to overcome the issues of vanishing or exploding gradients in traditional Recurrent Neural Networks (RNNs). By incorporating gating mechanisms (including input, forget, and output gates), LSTMs effectively manage and control the flow of information, allowing them to learn and remember long-term dependencies [32]. As of infectious diseases, long-term dependencies refer to the influence of past conditions on the current or future state of the disease spread. In epidemic simulation, LSTMs can predict future outbreak trends using historical infection data [33]. Nikparvar et al. used a multivariate LSTMs to predict infections and deaths in U.S. counties, enhancing accuracy by combining time-series and mobility data [34].

Understanding the spatio-temporal diffusion patterns of post-lockdown epidemics and the interactions between regions has become a crucial scientific issue. While various models and methods exist to study epidemic dynamics, most focus on single-dimensional analysis, primarily describing the impact of specific factors under strict control measures without effectively capturing regional

differences and interactions, such as socioeconomic factors variability across regions, as well as mobility-driven connections arising predominantly from human travel and transportation flows. In this study, we utilize a spatio-temporal model based on several modeling architectures. This model is designed to simulate the spread of epidemics and analyze their distribution when control measures are lifted, providing a multifactorial geographic analysis of the dynamics. Based on the multi-source spatio-temporal data of prefecture-level cities in China, this study uses GNNs to deal with the spatial dependence relationship in the complex network structure and constructs the edge weight considering the influence of human flow factors, so as to reflect the spatial connection and interaction between different regions. Additionally, LSTM was used to capture the characteristics of time series changes, and the dynamic development of the epidemic following the relaxation of control measures was effectively simulated and predicted. Through a comprehensive analysis of these interconnected factors, this study achieves an in-depth understanding of the dynamics and transmission patterns of epidemics.

Methods

Data collection

Epidemic data

This study utilized confirmed case data from different regions in China sourced from the Chinese Center for Disease Control and Prevention's fever clinic attendance records [35]. The data includes national and provincial totals of fever clinic visits, positive cases, and the positivity rate from December 12, 2022 to June 6, 2023. The number of positive cases in fever clinics can reflect the actual situation of virus transmission and the infection rate within communities, providing preliminary information on epidemic activities. This data is aggregated at the provincial level; therefore, to enhance the analysis with more detailed insights, the study additionally collected granular data from the Baidu search index, sourced from Baidu's search engine (https://index.baidu.com). Baidu search index is a data-sharing platform based on the massive behavioral data of Baidu's internet users and uses data searched by Baidu's users to calculate the search indices of different keywords over various time periods. By setting location and time parameters, the platform retrieves daily search data on specific keywords across PC and mobile devices, as well as aggregate search data, revealing the information that users are most interested in regarding certain topics. Li et al. found that Baidu index had high correlation with daily incidences, with coefficient greater than 0.89 [36]. Thus, for this study, the Baidu search index platform was chosen as the data source, and data on the combined search indices of keywords on both PC and mobile devices were obtained using web scraping techniques. In total, the study collected search index data related to the epidemic from 309 prefecture-level cities across China, spanning from January 1, 2023 to November 1, 2023.

Human mobility data

The human mobility data utilized in this research was sourced from the Baidu migration platform (http://qianxi.baidu.com). Baidu migration, based on the location-based services (LBS) of the Baidu Maps open platform, dynamically and instantly visualizes migration trajectories and characteristics. This includes migration scale indices (inflow index and outflow index) for different study areas, reflecting the scale of population moving in or out. This data represents the total number of people migrating into and out of cities within a day, allowing for horizontal comparisons between different cities. It also includes the proportion of Origin-Destination (OD) migration between different regions on specific dates, detailing the origins of migration and the percentage of the population that migrated to a specific area the day before, relative to the total migrating population, including the proportions for the top 100 cities. The cities ranked beyond the top 100 have a very small proportion and are therefore negligible. The data obtained multiplies the daily ratios of migration origins by the total migration scale of different cities on that day, ultimately used to determine the edge weights between different cities.

Transportation network data

The 2024 national road and network data for China was sourced from OpenStreetMap (OSM) (https://www.openstreetmap.org/). OSM is a highly detailed map data base whose data is open-source and freely available for download, offering a free global map database. The road network data within OSM includes railways and urban roads. The latest national vector data for China's 1st to 5th class river systems also comes from OSM, updated in the year 2023. This includes the super detailed water body data extracted from OSM in 2023, stored in shapefiles containing lines and polygons. The railway and urban road networks in China are depicted in Fig. 1a and b, while the 1st to 4th class water system networks are shown in Fig. 1c. Flight data for China was collected based on the Ctrip app (https://www.ctrip.com/). The data encompasses the routes between cities with airports, recorded daily from January 1 to January 7, 2022. The method involves querying flights between specific cities each day, recording the starting and ending cities for each route. The collected data reflects the network structure of flight routes across the country, as displayed in Fig. 2b, which illustrates the collected flight routes for all flights in China.

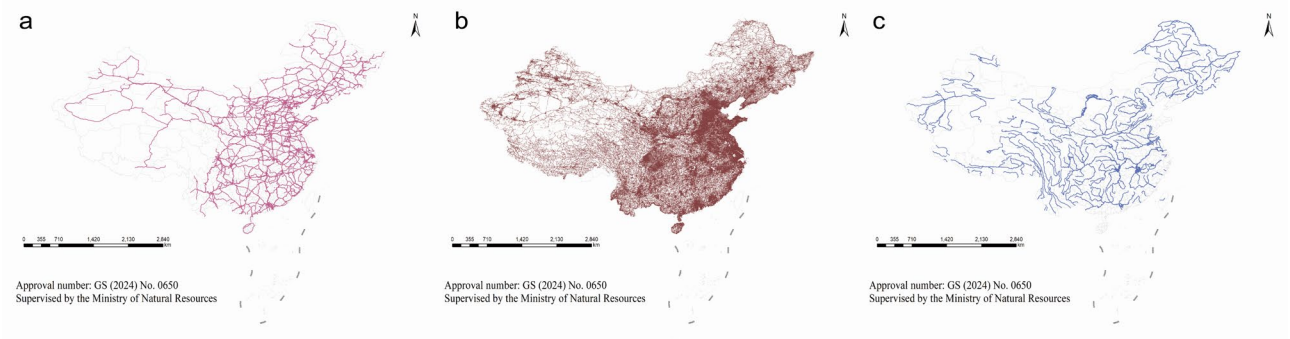

Fig. 1 The transportation network of China (Fig. 1**a** depicts the national railway network; Fig. 1**b** shows the national road network; Fig. 1**c** presents the national 1 st to 4th class water systems)

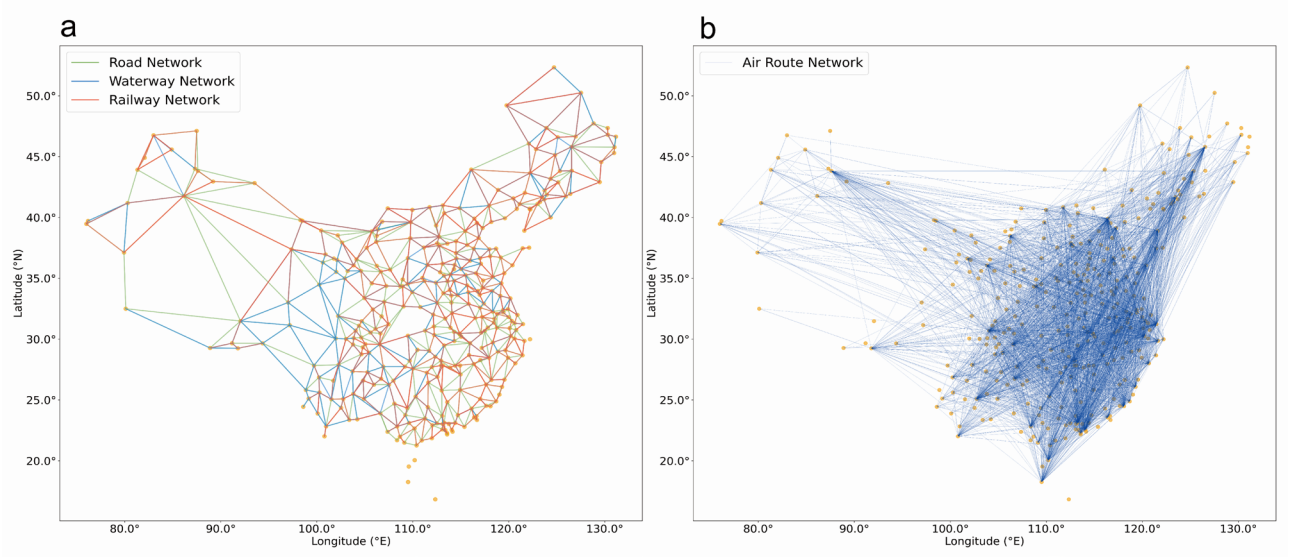

Fig. 2 Connectivity networks of various transportation modes in China (Fig. 2**a** represents the connectivity network of road, rail, and waterway transport; Fig. 2**b** shows the connectivity network of air transport)

Characteristic variables data

The feature variable data used in this analysis includes the population density of prefecture-level cities across China and GDP (Gross Domestic Product) data for each of these cities for the year 2022, both sourced from regional statistical bureaus of China. GDP data, as a key indicator of the economic output of a region, reflects the economic scale and development level of that area. Additionally, the study utilized nighttime light data, which provides spatial distribution information about artificial light sources on the earth's surface, revealing the intensity of human activity and regional development disparities. The national nighttime light data for prefecture-level cities was compiled from corrected DMSP-OLS and SNPP-VIIRS data, covering annual data from 1992 to 2023 for China [37]. The 2023 corrected nighttime light raster data were aggregated according to the administrative boundaries of China's prefecture-level cities, using the average nighttime light values as input features.

Study design

Construction of connectivity networks

To determine the connectivity between regions via transportation networks, we define direct connections based on the presence of transportation routes linking them. If a transportation network, such as a road or railway, extends between two regions, they are considered directly connected. In other words, regions are considered directly connected if there is a transportation network linking them; otherwise, they are not connected. This method provides a structured approach to capturing the real-world transportation connections that influence regional interactions and mobility patterns.

Using this retrieval method, we constructed connectivity networks covering various modes of transportation in China. Figure 2a displays the primary corridor network of cities formed by roadways, railways, and waterways. Figure 2b shows the distribution of all flight routes in China, including over 3000 routes. The flight data have

Table 1 Connectivity coverage of various transportation networks

Transportation Patterns	Number of Cities	Coverage
Road transportation	334	98.53%
Rail transportation	324	95.58%
Water transportation	297	87.61%
Air transportation	201	59.29%

Table 2 Baidu search indices of keywords retrieved

Cough, Amoxicillin, Pneumonia, Dry cough, Nasal congestion, COVID, COVID-19, High fever, Body temperature, Cough with phlegm, Gan Kang (Compound Paracetamol and Amantadine Hydrochloride Tablets), Fever, Lianhua Qingwen (Chinese patent drug), Common cold, Sore throat, SARS-CoV-2, Infection, Lianhua Qingwen (Chinese patent drug, another chinese expression), Coughing up phlegm, Pharyngeal pain, Contac, Tylenol, Fever clinic, Vaccine, Antibody, covid-19, Runny nose, Throat swelling and pain, Face mask, Cold symptoms, Headache, Throat pain, Cold medicine, Febrile, Shortness of breath, Epidemic, Novel pneumonia, Muscle soreness, Sneezing, Breathing difficulties, Cold cough, Disinfection, Influenza virus, Fatigue, Viral cold, Influenza, Flu symptoms, Diarrhea, Epidemic influenza, Immunity, Viral influenza, Cold with runny nose, Treatment, Flu vaccine, Flu epidemic, Tiredness

Searches were conducted in Chinese, and the above table includes translations of the key terms

been organized by origin and destination, which suffices for establishing clear adjacency relationships and requires no further retrieval.

The coverage of the connectivity network of various modes of transportation in China is shown in Table 1: Among the various transportation modes, air transportation has a coverage rate of 59.29%, followed by water transportation at 87.61%, railway transportation at 95.58%, and road transportation with the highest coverage at 98.53%. Such a connectivity network covers major cities in China, connecting virtually all cities and allowing for comprehensive analysis understanding on the interactions between regions.

Construction of epidemic spread indicators

This study first selected search terms related to the spread of the epidemic in terms of symptoms, treatment, and preventive measures, and then conducted a preliminary evaluation of each keyword in the data set to determine its relevance to the research topic. A total of 56 keywords were collected in the study, as shown in Table 2.

To further filter out highly correlated keywords, this study conducted a correlation analysis between the number of fever clinic cases and the organized Baidu search index of keywords. Initially, the correlation analysis was performed between the number of fever clinic cases in various regions and the Baidu search index of each keyword for the corresponding areas. This provided the correlation coefficients for different regions, which were then averaged to obtain the average correlation coefficient for each keyword. During the initial screening of keywords, the pearson correlation coefficient between the time series of selected keywords and the number of fever clinic cases should be at least 0.7, and all should pass the significance test. An analysis of the ranking of correlations between various keyword Baidu search indices and the epidemic revealed that 12 out of 56 keywords have a correlation coefficient greater than 0.7 with the epidemic, as shown in Table 3.

Table 3 Average correlation coefficients between the Baidu search indices of keywords and the number of fever clinic cases

Keyword Name	*R*	Keyword Name	*R*
Cough (V1)	0.8593	COVID (V7)	0.7732
Amoxicillin (V2)	0.8301	High fever (V8)	0.7607
Dry cough (V3)	0.7834	Cough with phlegm (V9)	0.7261
Pneumonia (V4)	0.7824	Body temperature (V10)	0.7250
Nasal congestion (V5)	0.7771	Gan Kang (V11)	0.7211
COVID-19 (V6)	0.7746	Fever (V12)	0.7054

In this study, we applied an exponential decay model to adjust the weights of keywords, ranking them in descending order based on their correlation scores, and assigning each keyword an initial weight based on its ranking. The weight of each keyword was adjusted using an exponential decay function $W_i = \exp(-\alpha \cdot \mathrm{rank}_i)$, where W_i represents the keyword weight, rank_i is the ranking of the keyword, and α is the decay coefficient, which controls the rate of weight reduction. In this study, α was set to 0.5. To ensure that the total sum of all keyword weights equals 1, all adjusted weights were normalized. The weighted sum of all keywords was then used to construct an index that reflects the dynamics of epidemic transmission. The final nationwide correlation coefficient achieved was 0.970, as shown in Fig. 3.

Construction of graph structures for GNNs

GNNs can effectively capture spatial dependencies and information hidden within non-Euclidean structural data, efficiently solving the spatio-temporal challenges associated with epidemic forecasting. A graph is the fundamental structure utilized by GNNs, defined as $G = (V, E, A)$, where V represents the set of vertices or nodes, E is the set of edges between nodes, and A is the adjacency matrix. Nodes and edges possess distinct attributes. In this work, a weighted undirected graph was defined within the model, with cities listed as a set of vertices V; the spatial relationships between cities are represented by the set of edges E, and the local attributes of cities (including time series data) are listed as a set of features X. Vertex attributes are divided into two categories: static attributes, which include population numbers, GDP, and nighttime lights; and dynamic attributes, which consist of the time series of epidemic spread dynamics indicators. All these variables undergo z-score normalization to ensure a uniform scale across different

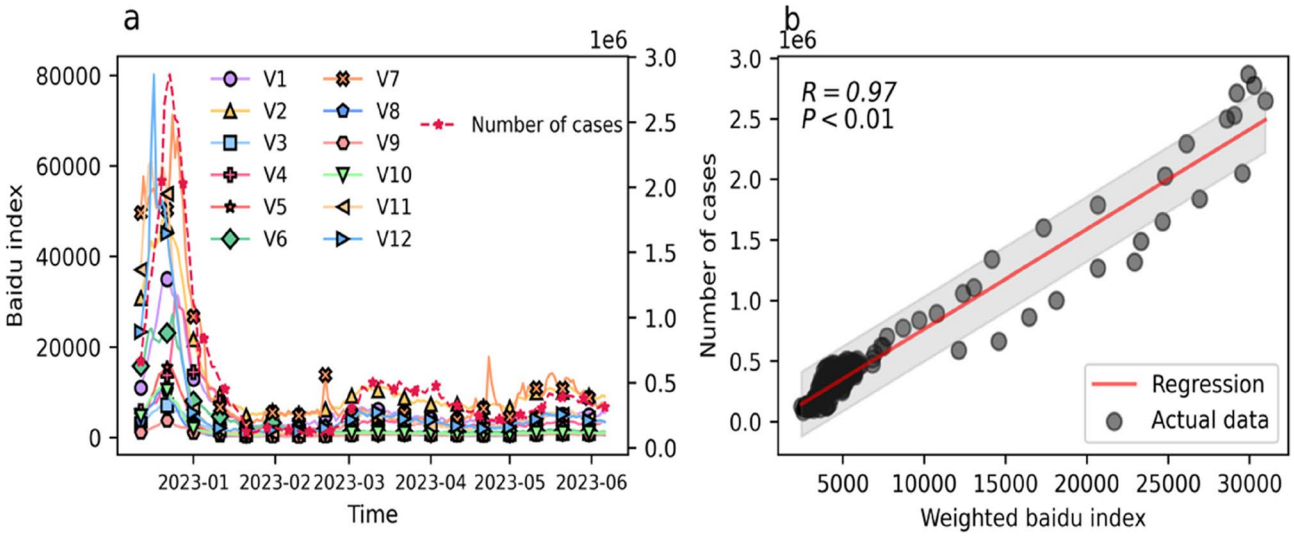

Fig. 3 The correlation between constructed epidemic spread indicators and epidemic transmission (Fig. 3**a** shows the time trend of the selected 12 Baidu search indices and the number of cases in national fever clinics; Fig. 3**b** represents the correlation between the number of cases in national fever clinics and the weighted Baidu search index)

regions. For the set of edges E, the adjacency matrix is crucial for capturing spatial dependencies. The adjacency matrix can be defined as a union of previously described connectivity grids, encompassing roadway, waterway, railway, and airline networks. In the study, edge weights were determined by the intensity of human mobility interactions and the physical distance between different regions, ultimately weighting the adjacency matrix to form a weighted connectivity matrix.

Construction of edge weights

Most previous studies have based GNNs edge weights primarily on physical distance, but this approach has limitations, as roads and traffic connections between regions often do not follow straight paths. Therefore, this study proposes a new method that more accurately reflects the actual interaction strength between cities by integrating both human mobility and physical distance between cities. Based on these factors, we have weighted the adjacency matrix to form a weighted connectivity matrix that reflects the effective strength of connections.

The defined edge weights in our model consider the intensity of human mobility interactions between regions. Given the availability of data over time, the study period selected for calculating human mobility edge weights is from January 1, 2023 to November 1, 2023. The average human traffic between two points during this period is used to determine the interactions of human mobility. The data period for calculating edge weights is as comprehensive as possible to cover the entire forecast period. The population ratio data are first processed by multiplying the ratio of the population migrating into (or out of) one city from another by the corresponding city's migration scale index on that day (this value represents the total number of people migrating into or out of that city in one day, allowing for horizontal comparisons between different cities). This value is then scaled up by a factor of 1000, which to some extent represents the population index of migration into (or out of) another city. The calculations are as shown in formulas (1–2):

$$\mathrm{MII}_{ij} = \mathrm{IPR}_{ij} \times \mathrm{ISI}_j \times 1000 \tag{1}$$

$$\mathrm{MOI}_{ij} = \mathrm{OPR}_{ij} \times \mathrm{OSI}_j \times 1000 \tag{2}$$

In the formulas, MII_{ij} represents the migration scale index of population moving in from region i to region j; IPR_{ij} is the ratio of the population size moving in from region i to region j; ISI_j is the migration scale index for region j at a given time for incoming populations; MOI_{ij} represents the migration scale index for population moving out from region i to region j; OPR_{ij} is the ratio of the population size moving out from region i to region j; OSI_j is the migration scale index for region j at a given time for outgoing populations.

Since the dataset includes daily data for the top 100 cities in terms of people moving in and out of the 309 cities, it first needs to be organized and preprocessed. For each pair of cities, we calculate the average daily migration scale for both incoming and outgoing populations within the selected date range. If a pair of cities does not rank in the top 100 on a particular day, the population flow for that pair is considered zero for that day. The variation in the daily top 100 rankings of incoming and outgoing cities has been partially addressed by averaging the data across all dates. Even if some cities are not

in the top 100 on certain days, this variation is smoothed out through the daily average calculation. Through these steps, a composite index reflecting the human traffic flow between cities is obtained, which can be used as the weight of edges in the graph model. Additionally, this study employs the min-max normalization method to normalize the data. Min-max normalization is a common data preprocessing technique that linearly transforms and scales each value in the original data to fit within a specified range, typically from 0 to 1. The specific transformation formula is shown as formula (3):

$$X' = (X - X_{\min})/(X_{\max} - X_{\min}) \tag{3}$$

In the formulas, X represents a specific value from the original data, and X' represents the normalized value. $X_{\min}$and $X_{\max}$ are the minimum and maximum values in the original data, respectively.

$$\text{flow}_{ij} = (\text{MII}_{ij} + \text{MOI}_{ij})/2 \tag{4}$$

$$\text{edf}_{ij} = e^{-\beta dist_{ij}} \tag{5}$$

$$W_{ij} = \alpha \times \text{norm}\ (\text{flow}_{\text{ij}}) + (1\text{-}\alpha) \times \text{norm}\ (\text{edf}_{ij}) \tag{6}$$

In this study, the edge weights are calculated by integrating the weighted interaction strength of human mobility with the distance decay function applied to the physical distance between regions (as defined in Eqs. 4–6). In these equations, W_{ij} represents the edge weight between node *i* and node *j*. Here, $(\text{MII}_{ij} + \text{MOI}_{ij})/2$ denotes the human traffic flow between node *i* and node *j*, where $\text{norm}\ (\text{flow}_{\text{ij}})$ is the normalized human mobility scale between city *i* and city *j*, and $\text{norm}\ (\text{edf}_{ij})$ is the normalization of the distance decay function applied to the physical distance between city i and city j.

We explicitly utilize an exponential decay function $e^{-\beta dist_{ij}}$ with β = 0.01 to model the diminishing interaction intensity with increasing distance [38]. Physical distances are calculated using latitude and longitude coordinates associated with each city center to weight the graph edges. In the calculation of edge weights, a weight of 0.5 is set, and using the above formulas, the weights between different nodes are constructed as shown in Fig. 4. By applying these edge weights to the adjacency matrix, a weighted adjacency matrix is created, which in

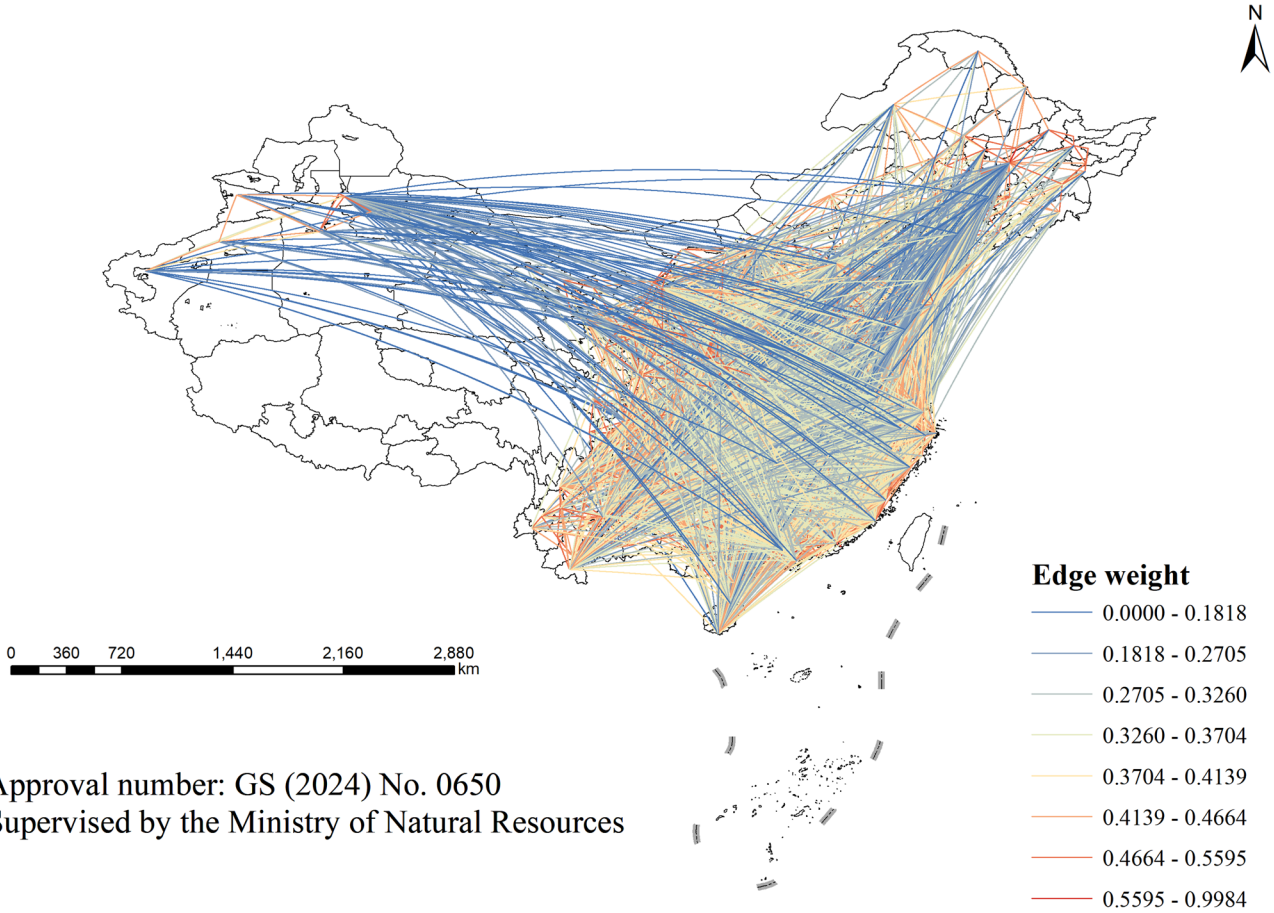

Fig. 4 Edge weights of the graph network connectivity matrix based on the intensity of human mobility interactions and physical distance

turn can reflect the intensity of interactions between different regions.

Spatio-temporal forecasting model architecture

Our forecasting model combines GNNs for spatial feature learning with LSTM network for temporal sequence modeling. The GNNs components are composed of a Graph Convolution Networks (GraphConv) layer followed by a Graph Attention Networks v2 (GATv2Conv) layer, and the output from these graph layers feeds into the LSTM. The GraphConv layer first aggregates information from neighboring cities to capture the general spatial structure of the mobility network. On top of this, we apply a GATv2Conv layer, which introduces an attention mechanism. The GATv2Conv layer computes learnable attention weights for each edge, so that important connections receive higher weights. In combination, GraphConv provides a broad propagation of information across the network, and GATv2Conv hones in on the most influential travel routes. The spatially informed node features are then passed into an LSTM to forecast epidemic dynamics over time. The LSTM is well-suited for this task because it can maintain long-term dependencies through its gated memory cells. In our model, the LSTM processes the sequence of graph-derived features and learns the evolution of the epidemic, outputting predictions for future infection counts in each city.

We modeled data from 309 cities across China, integrating a GNNs module and a recurrent network with an input time window to effectively manage long-term dependencies. The aggregation step involves collecting information from neighboring nodes and the update step updates the current node's state based on the information gathered during aggregation and the previous state. These steps are crucial for understanding patterns and trends in historical data. The model takes as input a composite feature matrix (covering both static and dynamic features) and a weighted adjacency matrix, maximizing the use of available historical information to enhance prediction accuracy. The prediction results are based on the next day's forecast within a T-day historical time window, ensuring the model can respond to recent data changes.

Model architecture implementation details

To ensure the model generalizes well and does not overfit to regions with extremely high mobility (high-flow connections), we incorporate two key techniques. These aim to mitigate any bias toward the busiest travel routes and encourage the model to learn broad patterns. We normalize the inter-city mobility weights using Min-Max scaling before inputting them to the GNNs. This normalization prevents extremely high-flow routes from skewing the learned spatial features, forcing the GNNs layers to consider relative differences more evenly. Additionally, We apply a dropout layer within the model, specifically on the graph layer outputs, to randomly omit a fraction of neurons during training. By randomly dropping out the units (rate = 0.01), the model cannot solely depend on the signals from high-mobility regions or particular pathways. Even regions with lower mobility thus get a chance to influence the training, improving generalization.

To evaluate the effectiveness of our model, we implemented a testing strategy that used a 7-day historical time window. Meanwhile, the data used in this study spanned from December 1, 2022 to September 26, 2023, comprising a 300-day time series divided into 6 folds for cross-validation, each including distinct training, testing, and validation sets. During model training, the dataset was segmented into these sets based on the timeline, with each subset defined as a partition of the time series from day one to dayθ_k, for 6-fold cross-validation. Each fold defined as a time interval starting from the first day of the epidemiological study and continuing up to dayθ_k, with $\theta_k$varying with each fold. This allowed the model to utilize time series of varying lengths starting from the first day of the epidemic, helping to assess whether the proposed architecture could capture dynamics within specific periods. The segmentation of data into folds was systematically adjusted to balance training, validation, and testing samples effectively, ensuring comprehensive learning and evaluation. Specifically, the size of the training set gradually increased from 90 days at k = 1 to 300 days at k = 6, while the sizes of the validation and testing sets were fixed at 30 days each. The dataset segmentation method is as shown in formulas (7–9).

$$\Sigma_{k,\text{train}} = [1, \ldots, \theta_k], \quad \theta_k = 90 + 30(k-1) \tag{7}$$

$$\Sigma_{k,\text{valid}} = [\theta_k + 1, \ldots, \theta_k + 30] \tag{8}$$

$$\Sigma_{k,\text{test}} = [\theta_k + 31, \ldots, \theta_k + 60] \tag{9}$$

We conducted a detailed cross-validation of the model architecture. To ensure the effectiveness of the proposed architecture, we first used the training set to fit the model and utilized the validation set for evaluation. This cross-validation method trained each fold of the model separately while comparing models via average loss. After evaluation, the model was refitted to the training and validation sets with the determined hyperparameters and then subjected to a final evaluation on a subset of the test set. In terms of model configuration, the following hyperparameters were set: the learning rate was set to 0.001, with a reduction to 0.25 of the original rate after every 200 epochs; the ADAM optimizer was used to optimize training and validation steps. Mean Square Error (MSE) and Mean Absolute Error (MAE) were used as

loss functions for backpropagation. Ultimately, to comprehensively evaluate the performance of the proposed architecture, we compiled the evaluation results of each model in their respective folds during the cross-validation process and calculated the average of these results. This approach verifies the performance of individual models and gauges the overall architecture's performance across multiple test scenarios, which is key to ensuring the model operates stably and achieves expected outcomes in practical applications.

Evaluation metrics

In this study, we comprehensively evaluated the effectiveness of the model by employing three core evaluation metrics that analyzed model performance from multiple perspectives. These assessments included urban agglomerations, provincial divisions, forecast time spans, and various data folds. The selected metrics include the Root Mean Squared Error (RMSE), Mean Absolute Error (MAE), and Mean Absolute Percentage Error (MAPE). The calculations are shown in formulas (10–12). Here,$\hat{y}_i$ represents the predicted value for the i-th observation,$y_i$represents the actual value for the i-th observation, and M is the number of values to be predicted.

$$\mathrm{RMSE}(\widehat{y}, y) = \sqrt{\frac{1}{M}\sum_{i=1}^{M}(y_i - \hat{y}_i)^2} \tag{10}$$

$$\mathrm{MAE}(\widehat{y}, y) = \frac{1}{M}\sum_{i=1}^{M}|y_i - \hat{y}_i| \tag{11}$$

$$\mathrm{MAPE}(\hat{y}, y) = \frac{1}{M}\sum_{i=1}^{M}\left|\frac{y_i - \hat{y}_i}{y_i}\right| \tag{12}$$

Results

Model training results

Training and validation losses across training epochs are depicted in Fig.A3 [see Additional file 1]. Additionally, the dataset was divided according to the timeline, with time series assigned to various folds, each fold defined as an independent segment of the time series. In this research, six-fold cross-validation (k = 1, 2, 3…6) was employed to ensure robustness and reliability of the evaluation results, and we analyzed the prediction errors across different folds, with the results displayed in Fig.A4 [see Additional file 1]. Cross-validation analysis revealed fluctuations in model performance across different folds, enabling adjustments to training parameters based on performance variations.

Model analysis results

The results of the third cross-validation, derived from the model established in the third training phase and trained using only half of the available time series data. Figure 5 systematically compares four geographically representative cities: Harbin (Northeastern region), Wuhan (Central region), Xiamen (Eastern region), and Xi'an (Western region). These case studies validate the model's adaptability across China's four major economic zones as defined in Fig.A2 [see Additional file 1]. For extended analysis at the urban cluster scale, Fig.A5 [see Additional file 1] further illustrates epidemic spread dynamics in main cities in three major urban agglomerations: the Beijing-Tianjin-Hebei region (BTH), the Yangtze River Delta (YRD), and the Pearl River Delta (PRD). The model's simulated predictions generally aligned with actual trends, demonstrating its effectiveness in capturing complex scenarios. Notably, towards the end of 2022, as lockdown measures were lifted, several cities experienced significant epidemic fluctuations. The first major outbreak occurred from December 2022 to the Spring Festival in 2023, primarily due to the rapid spread of the virus following sudden relaxations in preventive measures. This was followed by second and third peaks during March and Labour Day holiday in May, reflecting the impact of increased human mobility and social gatherings during holidays. The simulation results showed consistent epidemic patterns across cities, confirming the model's effectiveness and practicality.

Model analysis error

Based on the proposed methodology framework, we conducted a comprehensive analysis based on geographical location and levels of economic development (sourced from the National Bureau of Statistics of China), as economic development significantly reflects human mobility, which is crucial for understanding and predicting epidemic spread. As shown in Fig.A2 [see in Additional file 1], China's four major economic regions include the Eastern, Central, Western, and Northeastern regions, encompassing 85, 81, 108, and 35 prefecture-level cities respectively. As illustrated in Fig. 6, the prediction errors across the regions show a diverse pattern. This variation in the MAE, RMSE, and MAPE values across different regions may be influenced by various factors, including each region's economic development level and human mobility patterns. Regions like the Northeastern and Central areas, which exhibited smaller MAE and RMSE values, may benefit from certain characteristics. Conversely, the Western and Northeastern regions displayed larger MAPE values, suggesting variability that could be attributed to less uniform economic development and diverse mobility patterns. These discrepancies highlight how regional dynamics, such as population density and

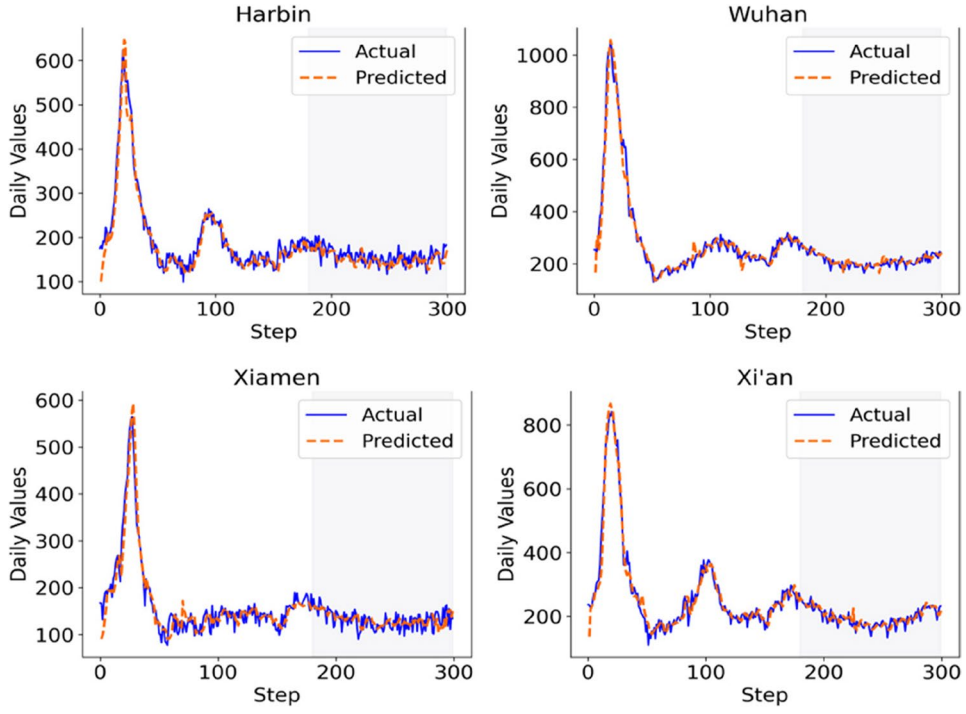

Fig. 5 Analysis results for epidemic spread dynamics in various cities (The orange dashed line represents predicted values, while the blue solid line represents actual values. The shaded areas represent the model's predictions for data that were not included during the training process), including Harbin (Northeastern region), Wuhan (Central region), Xiamen (Eastern region), Xi'an (Western region)

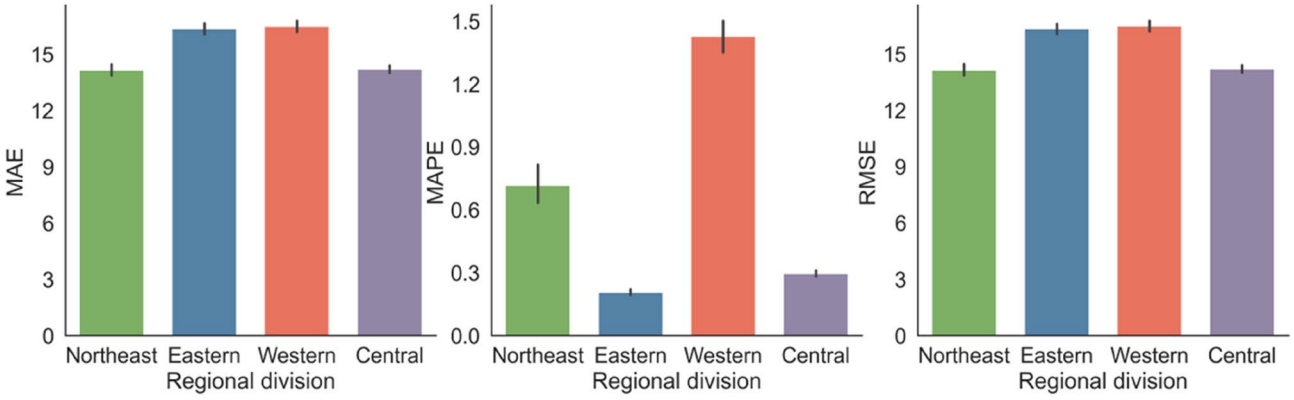

Fig. 6 Analysis errors for different regions in China (Northeastern, Eastern, Western, and Central regions), including MAE, MAPE and RMSE

economic activity, can impact the effectiveness of epidemic modeling and forecasting.

By using a time series segmentation approach, we ensured that the maximum testing period could cover up to 30 days, corresponding to the length of a single test set. We used three metrics for comparison to evaluate the performance of epidemic spread dynamics predictions over a range of 1–30 days. Fig.A6 [see in Additional file 1] displays the trend of loss functions over a 30-day prediction period across different divisions (Eastern, Central, Western, and Northeastern regions), where the error curves are based on the average loss values calculated from data across all folds and cities. The model's error metrics display a dynamic pattern across all regions. Initially, MAE and RMSE decrease, rise in the second week, and then decline to lower levels by the end of the 30-day period. Conversely, MAPE shows lower and stable levels in the Eastern and Central regions, while in the Western and Northeastern regions, it quickly drops in the first five days and then gradually decreases, stabilizing at a low level. These trends highlight the model's adaptability and underscore its potential for effective long-term epidemic forecasting across diverse geographic settings. Additionally, Fig.A7 [see in Additional file 1] offers a detailed display of predictive errors at the provincial level, emphasizing the spatial variability across different regions.

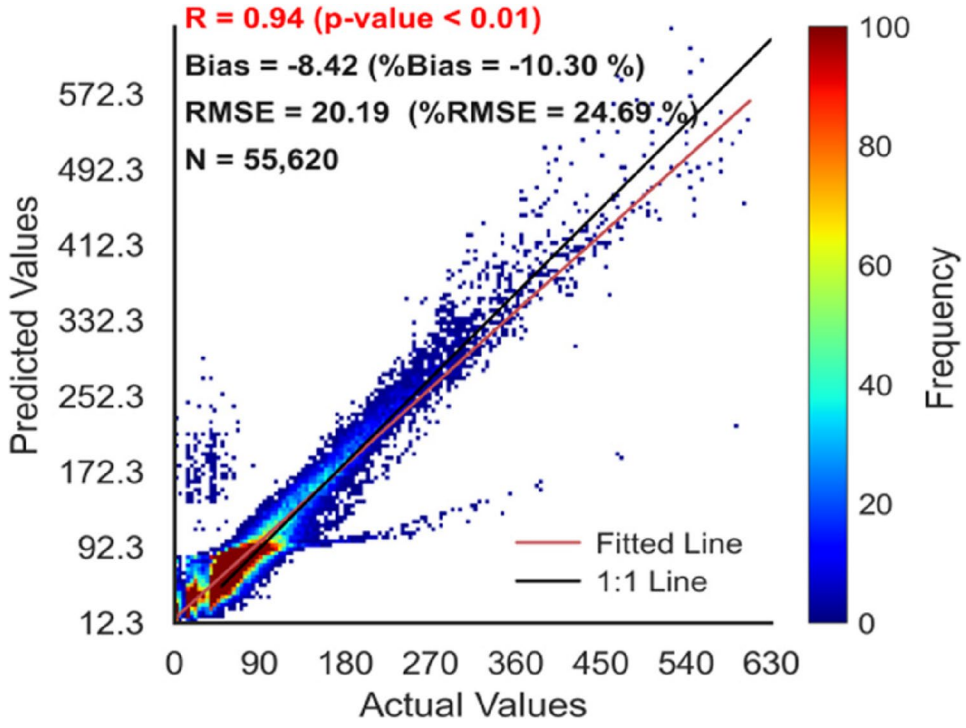

Fig. 7 Correlation between modeled and actual values across cities in China

Furthermore, at the prefecture-level city scale, the predictive errors for all 309 cities are shown in Fig. 7. The correlation coefficient between the model and the actual data reached 0.94, indicating high predictive accuracy. Moreover, the RMSE of 20.19, expressed as a dimensionless metric, further validates the model's effectiveness and reliability in practical applications.

Discussion

Our research yielded several important findings. The first is to enhance understanding of post-lockdown epidemic dynamics and modeling. Our spatio-temporal model effectively captures the rise, peak, and fall of epidemic transmission after lockdown is relaxed. It successfully modeled the resurgence patterns observed when restrictions were lifted, indicating that the model can reflect real-world epidemic trend changes in the aftermath of lockdown measures. Analysis suggests that human mobility and travel patterns were correlated with epidemic resurgence, in alignment with prior evidence emphasizing the importance of mobility in epidemic outbreak [6, 10]. Regions that experienced higher increases in mobility tended to see subsequent increases in epidemic activity, which our model was able to anticipate. This finding underscores the critical role of mobility in driving new infection waves, reinforcing previous findings that mobility metrics are critical for accurate outbreak predictions [22, 25, 26]. Unlike many prior studies that have primarily focused on single-region modeling, our results demonstrate consistent epidemic trends across multiple prefecture-level cities. In our case studies (in distinct economic areas), the model identified similar pattern dynamics, suggesting that it captured fundamental characteristics of epidemic spread that are not limited to a single city or region. The observed cross-region generalization suggests that our model captures fundamental transmission dynamics beyond localized outbreaks. This broader applicability addresses an important yet often overlooked aspect in epidemic modeling, where regional differences and interactions have often been inadequately explored or omitted [39, 40], particularly for fine-scale simulations at the prefecture-level cities in China following the lifting of control measures. Our results indicate that the learned patterns are broadly applicable, enhancing the model's relevance to diverse settings. Therefore, the capacity of our proposed method to generalize spatially represents a improvement over conventional region-specific models, making our findings particularly relevant for diverse geographic contexts.

The strengths of the GNNs lie in its ability to perform complex simulations based on local (vertex) and structural (edge) features, guiding future research to focus on dynamically adjusting adjacency matrix weights with machine learning to reflect policy changes, developing refined geospatial tools for predicting virus spread in smaller areas, and enhancing a predictor architecture that processes a broad range of time-series data for widespread application in public health studies. The model's

ability to incorporate mobility data means it can serve as an early warning system for epidemic resurgences. In practice, surges in travel and movement often precede rises in cases. By detecting these mobility upticks and accurately forecasting the consequent case increases, public health authorities could receive advanced notice of an impending outbreak. Our results highlight the value of integrating human mobility metrics into epidemic forecasting, which can directly inform policy. By simulating different mobility scenarios through the model, decision-makers can quantitatively assess the potential impact of policy choices on future case counts. Because our approach proved effective across different metropolitan areas and even across countries, it offers a general framework that agencies in various locales could adopt. Moreover, the framework could be adapted to other infectious diseases where human mobility drives spread (for example, influenza or dengue fever in interconnected communities).

The research still has some limitations, such as not distinguishing the specific impacts of different transportation modes, which could limit its accuracy in certain scenarios. While it has shown good predictive performance across multiple cities and regions, its generalizability needs further verification across a broader geographic scope. Its accuracy currently relies on economic and human mobility data, whose updating frequency and coverage limitations could hinder further precision improvements. The granularity of transportation and mobility data crucially affects the predictive accuracy of our model. In regions like the Western part of China, where transportation data might be sparser and less regular, the coarser granularity could lead to less accurate predictions. Moreover, the model has yet to fully consider complex factors like policy changes, public health emergency measures, and population compliance, which might affect the accuracy and practicality of its predictions. Future work will comprehensively extend and deepen this research by exploring diverse data sources, including social media and mobile phone signals, to gather more real-time information on human mobility and public sentiment. It will also integrate multiple data sources like weather conditions, traffic flows, and medical resource distribution to enhance the model's adaptability to environmental variables. Additionally, further efforts will involve developing dynamic adjustment mechanisms for the model to adapt to policy changes and public health interventions, combining predictive models with decision-support systems to provide real-time epidemic trend predictions and resource allocation recommendations for government and public health institutions, and exploring the model's potential applications in vaccine distribution and emergency response planning, all of which will significantly enhance the model's practicality and impact.

Conclusions

This study employs a spatio-temporal model that utilizes deep learning models to accurately simulate the dynamics of epidemic spread across various prefecture-level cities in China. This model utilizes a traffic-based graphical representation to depict the intensity of human mobility interactions between regions, employing GNNs and time-series neural networks to analyze both spatial dependencies and temporal trends. Extensive cross-validation and error analysis show that the model performs well across various urban clusters with a high correlation coefficient and notably reduced error results. Over a 300-day period, the model demonstrated adaptability across different temporal windows and its value for long-term forecasting, critical for public health decision-making and resource allocation. Collectively, these findings demonstrate that our approach can reliably model complex epidemic behaviors in an interconnected, post-lockdown context. By capturing how increased mobility leads to case surges and doing so across varied regions, it provides empirical evidence that combining human mobility networks with advanced neural architectures can generalize across different settings. The study not only deepens understanding of epidemic transmission mechanisms but also provides a scientific basis for public health strategy, particularly in optimizing resource allocation and epidemic control measures.

Abbreviations

COVID-19	coronavirus disease 2019
SEIR	Susceptible-Exposed-Infectious-Recovered
GNNs	Graph Neural Networks
GraphConv	Graph Convolution Networks
GATv2Conv	Graph Attention Networks v2
LSTMs	Long Short-Term Memory Networks
RNNs	Recurrent Neural Networks
OSM	OpenStreetMap
GDP	Gross Domestic Product
LBS	location-based services
OD	Origin-Destination
MLP	Multilayer Perceptron
MSE	Mean Square Error
MAE	Mean Absolute Error
RMSE	Root Mean Squared Error
MAPE	Mean Absolute Percentage Error
BTH	the Beijing-Tianjin-Hebei region
YRD	the Yangtze River Delta
PRD	the Pearl River Delta

Supplementary Information

The online version contains supplementary material available at https://doi.org/10.1186/s12879-025-11708-6.

Supplementary Material 1. Additional file 1: Supplementary figures related to this article

Supplementary Material 2. Additional file 2: Dataset and materials related to this article

Acknowledgements
The authors acknowledge the Chinese Center for Disease Control and Prevention for providing data on cases from fever clinics.

Authors' contributions
H. Li: Conceptualization, Data curation, Formal analysis, Investigation, Methodology, Validation, Visualization, Writing – original draft; J. Huang: Funding acquisition, Methodology, Project administration, Resources, Software, Supervision, Writing – original draft; W. Yan: Validation, Formal analysis, Data curation, Software, Writing – review and editing; Z. Hao: Validation, Formal analysis, Data curation, Writing – review and editing; R. Wang: Validation, Data curation, Writing – review and editing; Y. Zhao: Software, Formal analysis, Writing – review and editing; S. Hu: Conceptualization, Methodology; X. Lian: Software, Resources; L. Li: Resources, Supervision; All of the authors contributed to the discussion and interpretation of the manuscript. All authors read and approved the final manuscript.

Funding
This work was supported by the National Key Research and Development Program of China (2023YFC3503400), the Self-supporting Program of Guangzhou Laboratory (SRPG22-007), the Major Project of Guangzhou National Laboratory (GZNL2024A01004), and the Gansu Province Intellectual Property Program (Oriented Organization) Project (22ZSCQD02).

Data availability
All data generated or analyzed during this study are included in this published article [and its supplementary information files].
Data supporting the findings of this study are derived from several sources. The confirmed case data from the Chinese Center for Disease Control and Prevention, including fever clinic attendance records, cannot be made public due to privacy concerns. Publicly accessible data used in the study include Baidu search index data (https://index.baidu.com), 2024 national road and network data from OpenStreetMap (https://www.openstreetmap.org/), flight data from the Ctrip app (https://www.ctrip.com/), population density and GDP data from regional statistical bureaus (https://www.stats.gov.cn/sj/ndsj/), corrected nighttime light data for 1992 to 2023 (https://doi.org/10.1109/TGRS.2021.3135333), and human mobility data from the Baidu migration platform (http://qianxi.baidu.com). And the relevant data and codes of this study can be provided according to reasonable requirements.

Declarations

Ethics approval and consent to participate
According to the local legislation and institutional requirements, ethical review and approval is not required for this study. The data involved in the manuscript are collected from publicly available sources. Consent to participate in the study is not required, as all data used are in the public domain.

Consent for publication
Consent for publication is not applicable, as the manuscript does not include details, images, or videos relating to an individual person.

Competing interests
The authors declare no competing interests.

Received: 8 November 2024 / Accepted: 16 September 2025
Published online: 13 October 2025

References

1. Nicola M, Alsafi Z, Sohrabi C, Kerwan A, Al-Jabir A, Iosifidis C, et al. The socio-economic implications of the coronavirus pandemic (COVID-19): a review. Int J Surg. 2020;78:185–93.
2. Jain N, Hung IC, Kimura H, Goh YL, Jau W, Huynh KLA, Huy NT. The global response: how cities and provinces around the Globe tackled covid-19 outbreaks in 2021. Lancet Reg Health Southeast Asia. 2022;4:2772-3682.
3. Huang J, Zhang B, Wang D, et al. New direction of cross-disciplines in the 21st century: climate change and major epidemic monitoring and early warning. J Lanzhou Univ (Med Sci). 2022;48(11):1–3.
4. Huang J, Wang D, Zhu Y, Yang Z, Yao M, Shi X, Li H. An overview for monitoring and prediction of pathogenic microorganisms in the atmosphere. Fundam Res. 2023;4(3):430-41.
5. Lian X, Huang J, Li H, He Y, Ouyang Z, Fu S, et al. Heat waves accelerate the spread of infectious diseases. Environ Res. 2023;231:116090.
6. Jia JS, Lu X, Yuan Y, Xu G, Jia J, Christakis NA. Population flow drives spatio-temporal distribution of COVID-19 in China. Nature. 2020;582(7812):389–94.
7. Huang J, Liu X, Zhang L, Zhao Y, Wang D, Gao J, et al. The oscillation-outbreaks characteristic of the COVID-19 pandemic. Natl Sci Rev. 2021;8(8):nwab100.
8. van Oosterhout C, Hall N, Ly H, Tyler KM. COVID-19 evolution during the pandemic–implications of new SARS-CoV-2 variants on disease control and public health policies. Virulence. 2021;12(1):507–8.
9. Department of Publicity. National Health Commission of the People's Republic of China. http://www.nhc.gov.cn/xcs/. Accessed 22 Jul 2023.
10. Kraemer MU, Yang CH, Gutierrez B, Wu CH, Klein B, Pigott DM, et al. The effect of human mobility and control measures on the COVID-19 epidemic in China. Science. 2020;368(6490):493–7.
11. Lai S, Ruktanonchai NW, Zhou L, Prosper O, Luo W, Floyd JR, et al. Effect of non-pharmaceutical interventions to contain COVID-19 in China. Nature. 2020;585(7825):410–3.
12. Ndlovu M, Mpofu MA, Moyo RG. Modeling COVID-19 infection in high-risk settings and low-risk settings. Physics and Chemistry of the Earth, Parts A/B/C. 2022;128:103288.
13. Xie Z, Qin Y, Li Y, Shen W, Zheng Z, Liu S. Spatial and temporal differentiation of COVID-19 epidemic spread in mainland China and its influencing factors. Sci Total Environ. 2020;744:140929.
14. Zargari F, Aminpour N, Ahmadian MA, Samimi A, Saidi S. Impact of mobility on COVID-19 spread–a time series analysis. Transp Res Interdiscip Perspect. 2022;13:100567.
15. Zheng R, Xu Y, Wang W, Ning G, Bi Y. Spatial transmission of COVID-19 via public and private transportation in China. Travel Med Infect Dis. 2020;34:101626.
16. National Institute for Viral Disease Control and Prevention, Chinese CDC. China Influenza Surveillance Weekly Report. https://ivdc.chinacdc.cn/cnic/zyzx/lgzb/202301/P020230129523264982112.pdf.
17. He S, Peng Y, Sun K. SEIR modeling of the COVID-19 and its dynamics. Nonlinear Dyn. 2020;101:1667–80.
18. Huang J, Liu X, Zhang L, Yang K, Chen Y, Huang Z, Wang D. The amplified second outbreaks of global COVID-19 pandemic. medRxiv. 2020. https://doi.org/10.1101/2020.07.15.20154161.
19. Liu X, Huang J, Li C, Zhao Y, Wang D, Huang Z, et al. The role of seasonality in the spread of COVID-19 pandemic. Environ Res. 2021;195:110874.
20. Huang J, Zhao Y, Yan W, Lian X, Wang R, Chen B, et al. Multi-source dynamic ensemble prediction of infectious disease and application in COVID-19 case. J Thorac Dis. 2023;15(7):4040.
21. Huang J, Zhang L, Chen B, Liu X, Yan W, Zhao Y, et al. Development of the second version of Global Prediction System for Epidemiological Pandemic. Fundam Res. 2024;4(3):516–26.
22. Yang Z, Zeng Z, Wang K, Wong SS, Liang W, Zanin M, et al. Modified SEIR and AI prediction of the epidemics trend of COVID-19 in China under public health interventions. J Thorac Dis. 2020;12(3):165.
23. Li H, Huang J, Lian X, Zhao Y, Yan W, Zhang L, Li L. Impact of human mobility on the epidemic spread during holidays. Infect Disease Modelling. 2023;8(4):1108–16.
24. Akuno AO, Ramírez-Ramírez LL, Espinoza JF. Inference on a multi-patch epidemic model with partial mobility, residency, and demography: case of the 2020 COVID-19 outbreak in Hermosillo. Mexico. Entropy. 2023;25(7):968.
25. Zhou Y, Xu R, Hu D, Yue Y, Li Q, Xia J. Effects of human mobility restrictions on the spread of COVID-19 in Shenzhen, China: a modelling study using mobile phone data. Lancet Digit Health. 2020;2(8):e417-24.
26. Du B, Zhao Z, Zhao J, Yu L, Sun L, Lv W. Modelling the epidemic dynamics of COVID-19 with consideration of human mobility. Int J Data Sci Anal. 2021;12(4):369–82.
27. Hu Z, Wu Y, Su M, Xie L, Zhang A, Lin X, Nie Y. Population migration, spread of COVID-19, and epidemic prevention and control: empirical evidence from China. BMC Public Health. 2021;21:1–12.
28. Wu S, Fan X, Chen L, Cheng M, Wang C. Predicting the spread of covid-19 in china with human mobility data. In Proceedings of the 29th International

Conference on Advances in Geographic Information Systems. Beijing: Association for Computing Machinery; 2021. p. 240–243.
29. Scarselli F, Gori M, Tsoi AC, Hagenbuchner M, Monfardini G. The graph neural network model. IEEE Trans Neural Networks. 2008;20(1):61–80.
30. Panagopoulos G, Nikolentzos G, Vazirgiannis M. Transfer graph neural networks for pandemic forecasting. In Proc AAAI Conf Art Intell. 2021;35(6):4838–45.
31. Oliveira LC, Oliva JT, Ribeiro MH, Teixeira M, Casanova D. Forecasting the COVID-19 space-time dynamics in Brazil with convolutional graph neural networks and transport modals. IEEE Access. 2022;10:85064–79.
32. Hochreiter S, Schmidhuber J. Long short-term memory. Neural Comput. 1997;9(8):1735–80.
33. Chimmula VKR, Zhang L. Time series forecasting of COVID-19 transmission in Canada using LSTM networks. Chaos Solitons Fractals. 2020;135:109864.
34. Nikparvar B, Rahman MM, Hatami F, Thill JC. Spatio-temporal prediction of the COVID-19 pandemic in US counties: modeling with a deep LSTM neural network. Sci Rep. 2021;11(1):21715.
35. Chinese Center for Disease Control and Prevention. Nationwide Epidemic Situation of COVID-19 Infections. https://www.chinacdc.cn/jksj/xgbdyq/. Accessed 22 Jul 2024.
36. Li C, Chen LJ, Chen X, Zhang M, Pang CP, Chen H. Retrospective analysis of the possibility of predicting the COVID-19 outbreak from internet searches and social media data. China 2020 Eurosurveillance. 2020;25(10):2000199.
37. Wu Y, Shi K, Chen Z, Liu S, Chang Z. Developing improved time-series DMSP-OLS-like data (1992–2019) in China by integrating DMSP-OLS and SNPP-VIIRS. IEEE Trans Geosci Remote Sens. 2021;60:1–14.
38. Chen zhuo. Jin fengjun, Yang yu, Wang wei. Distance-decay pattern and Spatial differentiation of expressway flow: an empirical study using data of expressway toll station in Fujian Province[J]. Progress Geogr. 2018;37(8):1086–95.
39. O'Sullivan D, Gahegan M, Exeter DJ, Adams B. Spatially explicit models for exploring COVID-19 lockdown strategies. Trans GIS. 2020;24(4):967–1000.
40. Macías RZ, Gutiérrez-Pulido H, Arroyo EAG, González AP. Geographical network model for COVID-19 spread among dynamic epidemic regions. Math Biosci Eng. 2022;19(4):4237–59.

Publisher's Note